Proximity of Transmembrane Segments M3 and M1 of the α Subunit of Na^+,K^+-ATPase Revealed by Specific Oxidative Cleavage Mediated by a Complex of Cu^{2+} Ions and 4,7-Diphenyl-1,10-phenanthroline†

Daniel M. Tal,‡ Juan M. Capasso,§ Keith Munson,|| and Steven J. D. Karlish*,‡

Department of Biological Chemistry, Weizmann Institute of Science, Rehovot 76100, Israel, University of Colorado Health Science Center, Denver, Colorado 80262, and Membrane Biology Laboratory, West Los Angeles VA Medical Center, Los Angeles, California 90073

Received June 6, 2001; Revised Manuscript Received August 16, 2001

ABSTRACT: This paper describes a novel approach to specific oxidative cleavage of Na^+,K^+-ATPase, mediated by Cu^{2+} ions and a hydrophobic phenanthroline, 4,7-diphenyl-1,10-phenanthroline (DPP), in the presence of ascorbate and H_2O_2. The cleavage produces two major fragments of the α subunit, with apparent molecular masses of 96.5 and 76 kDa, and N-termini near the cytoplasmic entrance of transmembrane segments M1 and M3, respectively, The kinetics indicate that both cleavages are mediated by a single Cu^{2+}−DPP complex. We infer that M3 and M1 are in proximity near the cytoplasmic surface. The yields of 96.5 and 76 kDa fragments are not significantly affected by ligands that stabilize different E_1 and E_2 conformations. In E_2(K) and E_2P conformations, a minor 5.5 kDa fragment with its N-terminus in M10 is also observed. The 96.5 and 76 kDa fragments are indistinguishable from two fragments near M3 and M1 produced by Fe^{2+}-catalyzed cleavage described previously [Goldshleger, R., and Karlish, S. J. D. (1999) *J. Biol. Chem. 274*, 16213−16221], whereas other Fe^{2+}-catalyzed cleavage fragments in the cytoplasmic P and A domains are not observed with the Cu^{2+}−DPP complex. These findings provide experimental support for the concept of two separate Fe^{2+} sites. A homology model, with Na^+,K^+-ATPase residues within transmembrane segments and connecting loops substituted into the crystal structure of Ca^{2+}-ATPase, shows the proximity between the sequences HFIH in M3 and EVWK in M1, near the cytoplasmic surface. Thus, the model strongly supports the conclusions based on cleavages mediated by the Cu^{2+}−DPP complex (or Fe^{2+} at site 2). As a corollary, the cleavages provide evidence for similar packing of M1 and M3 of Na^+,K^+-ATPase and Ca^{2+}-ATPase.

The Na^+,K^+-ATPase actively transports three Na^+ ions and two K^+ ions for each molecule of ATP hydrolyzed and is responsible for maintaining the normal transmembrane gradients of Na^+ and K^+ ions which are essential for the life of the cell.

By comparison with our extensive knowledge of the kinetics and function of Na^+,K^+-ATPase, our knowledge of molecular structure lags far behind (*1*, *2*). The recent publication of the 2.6 Å crystal structure of the related sarcoplasmic reticulum Ca^{2+}-ATPase is beginning to redress the balance since the structure has outstanding explanatory and predictive qualities with respect to all P-type pumps (*3*). Presumably, the tertiary structures of other P-type pumps resemble that of Ca^{2+}-ATPase, particularly within conserved cytoplasmic domains, but may show detailed differences related to the cation specificities, and for Na^+,K^+-ATPase and H^+,K^+-ATPase may show differences related to the presence of a β subunit (*4*, *5*). Of particular relevance in the present context, the Ca^{2+}-ATPase structure confirms the existence of 10 transmembrane helices deduced for Ca^{2+}-, Na^+,K^+-, H^+,K^+-, and H^+-pumps by biochemical techniques (*6*), but there are several unexpected features, including unraveling of sections of the M4 and M6 membrane-spanning helices that are involved in occluding Ca^{2+} ions. The details of Ca^{2+} occlusion sites within M4−M6 and M8 predicted from extensive mutagenesis studies (*7*, *8*) fit well with the structure.

This paper is concerned with the organization of transmembrane helices of Na^+,K^+-ATPase. The assumption that the organization of transmembrane helices of other P-type pumps is similar to that of the Ca^{2+}-ATPase is a good initial hypothesis, but particularly for pumps with more than one subunit, there might be differences in the helix arrangement of the α subunit in the region of subunit contacts. The β subunit of Na^+,K^+-ATPase and H^+,K^+-ATPase, which is required for stabilization of the α subunit and passage from the cell interior to the outer membrane (*4*, *5*, *9*, *10*), is known to interact with the α subunit in the region of transmembrane segment M8 (*9*, *10*). In addition, the renal Na^+,K^+-ATPase also contains a small single transmembrane protein, the γ subunit, which is a tissue-specific regulator and must also

† Supported by a grant from the Israel Science Foundation (15/00-1). A visit of J.M.C. to the Weizmann Institute was supported by the Weizmann Institute Renal Research Fund.

* To whom correspondence should be addressed. Telephone: 972 8 934 2278. Fax: 972 8 934 4118. E-mail: Steven.Karlish@weizmann.ac.il.

‡ Weizmann Institute of Science.

§ University Colorado Health Science Center.

|| West Los Angeles VA Medical Center.

10.1021/bi011167n CCC: $20.00
Published on Web 09/27/2001

interact with the α subunit (*11*). Thus, direct experimental evidence of helix packing is required to complement the Ca^{2+}-ATPase structural data, until such time when (or if) the structure of Na^+,K^+-ATPase itself becomes available.

We have made an initial attempt to obtain evidence of helix packing of Na^+,K^+-ATPase based on covalent cross-linking of the fragments of "19 kDa membranes" (*12*, *13*). The 19 kDa membranes are the products of extensive tryptic digestion of renal Na^+,K^+-ATPase, which removes ~50% of the protein but leaves well-defined membrane-embedded fragments, corresponding to M1/M2, M3/M4, M5/M6, and M7−M10, and essentially intact β and γ subunits. The 19 kDa membranes have the important feature of retaining the capacity for K^+ and Na^+ occlusion and ouabain binding, although ATP binding sites are digested away. Due to the intactness of the cation and ouabain sites, one can assume that the native organization of transmembrane helices is retained. Cross-linking with *o*-phthalaldehyde or Cu^{2+}−phenanthroline-induced S−S bridge formation revealed a number of proximities between fragments which, together with other information, led to formulation of an approximate model of helix packing (*14*, *15*). However, the difficulty of finding specific cross-linking reagents and analyzing the cross-linked peptides limits the value of this approach. Use of recombinant Na^+,K^+-ATPase and engineering of specific S−S bridging sites could be more fruitful.

Recently, we have introduced a technique of specific oxidative cleavage of renal Na^+,K^+-ATPase, which utilizes Fenton chemistry of bound transition metals such as Fe^{2+} or Cu^{2+} or metal complexes such as the ATP−Fe^{2+} complex. Addition of ascorbate with H_2O_2 generates OH radicals (or the reactive metal−peroxyl intermediates) at the bound metal site and cleaves the nearby polypeptide chain (*16*−*21*). Because more than one peptide bond can be cleaved from the same metal site, the technique has the important feature of providing information about the proximity of cleaved segments in the native protein, that is, their spatial organization. The properties of cleavages catalyzed by free Fe^{2+} or ATP−Fe^{2+} complexes are described in the original papers (*16*, *19*, *20*) and a recent review (*21*). In particular, these cleavages have provided evidence for large movements in the N, P, and A cytoplasmic domains, accompanying $E_1 \rightarrow E_2$ and $E_1P \rightarrow E_2P$ conformational changes and also a change in ligation of Mg^{2+} ions between E_1P and E_2P. The conclusions fit well with inferences on conformation-dependent domain movements from the reported Ca^{2+}-ATPase structure, which is in an E_1 conformation (*3*). We have surmised, mainly on the basis of the Ca^{2+}-ATPase structure, that there are two sites for binding of free Fe^{2+} (*21*), which is of immediate relevance to the work presented here. The first site (site 1) involves highly conserved residues in the P domain (denoted as nr.CSDK, nr.MVTGD, and VNDS) and A domain (TGES), and is highly sensitive to $E_1 \rightarrow E_2$ conformations. The second site for free Fe^{2+} (site 2) is located near the entrance of transmembrane segments M3 (involving an HFIH sequence) and M1, and is insensitive to conformations. Nevertheless, direct experimental evidence is lacking. In a separate study, free Cu^{2+} ions were found to catalyze specific cleavages of both the α and β subunits at the extracellular surface (*18*). These results provided significant constraint on the way models of helix packing can be constructed (*15*).

The results reported in this paper present a novel application of the cleavage technique. Normally, when an excess of a metal chelator, such as EDTA, is added to the incubation medium containing Fe^{2+} or Cu^{2+} ions, the free metal ion concentration is reduced to a negligible value, and all cleavages are suppressed. In contrast, addition of different phenanthroline derivatives to a reaction medium containing Cu^{2+} ions has been found to induce new cleavages. Here, we explore this phenomenon, showing that with the appropriate hydrophobic phenanthroline (DPP),[1] cleavages mediated by a Cu^{2+}−DPP complex are highly selective. This provides a way to detect proximities between transmembrane segments.

EXPERIMENTAL PROCEDURES

Enzyme Preparations. Na^+,K^+-ATPase (13−18 units/mg of protein) was prepared from pig kidneys, assayed, and stored at −20 °C in a solution of 250 mM sucrose, 25 mM histidine (pH 7.4), and 1 mM EDTA, as described in ref *22*. Prior to use, membranes were washed twice and suspended in a buffer solution containing 10 mM Tris-HCl (pH 7.5). Rat axolemma microsomes (2−3 units/mg of enzyme) prepared as described in ref *23* was a gift of R. Blostein.

Cleavage Reaction. Membrane suspensions (1 mg of protein/mL) were pre-equilibrated for 15 min with DPP or another phenanthroline derivative and $CuCl_2$ at the indicated concentrations, and incubated at 20 °C for the indicated times with freshly prepared solutions of 4 mM ascorbate (Tris) with 4 mM H_2O_2. To arrest the cleavage reaction, 10 μL of the 5-fold concentrated gel sample buffer also containing 10 mM EDTA and 5 mM desferal was added and samples were applied to gels.

Gel Electrophoresis, Blotting to PVDF, Immunoblots, and Sequencing. Procedures for running of 7.5 or 10% Tricine SDS−PAGE, including precautions prior to sequencing, semidry electroblotting to PVDF paper, immunoblots, and microsequencing of fragments, have been described previously in detail (*13*, *24*). Immunoblots (3−5 μg of protein per lane) were probed with anti-KETYY which recognizes the C-terminus of the α subunit ($K^{1012}-Y^{1016}$), except for the experimental results depicted in Figure 5 which also used "anti-M1/M2", prepared from a 11.7 kDa fragment ($D^{68}-R^{168}$), containing transmembrane segments M1 and M2 (*13*, *24*). Immunoblots were developed by enhanced chemiluminescence (ECL) using anti-rabbit IgGHRP conjugate and the protocol supplied with ECL reagents from the 1998 Amersham-Pharmacia Life Science Products catalog. Where fragments were to be sequenced, cleaved enzyme (1 mg/mL) was extracted with the nonionic detergent $C_{12}E_{10}$ (polyoxyethylene 10-lauryl ether), to remove contaminant proteins, prior to application to long 10% gels, and staining with Coomassie blue (see ref *16*).

Computer Modeling. A homology-based model for the membrane domain of the Na^+,K^+-ATPase α subunit was

[1] Abbreviations: H_2O_2, hydrogen peroxide; desferal, desferrioxamine mesylate; DEPC, diethyl pyrocarbonate; DPP, 4,7-diphenyl-1,10-phenanthroline; TMP, 3,4,7,8-tetramethyl-1,10-phenanthroline; neocuproine, 2,9-dimethyl-1,10-phenanthroline; phenanthroline, 1,10-*o*-phenanthroline; DPP-DS, 4,7-diphenyl-1,10-phenanthrolinedisulfonic acid; DMDPP, 2,9-dimethyl-4,7-diphenyl-1,10-phenanthroline; DMF, dimethylformamide.

Table 1: Residues of the Membrane Domain of the Ca^{2+}-ATPase Substituted with Residues of the Na^+,K^+-ATPase for Generation of the Homology Model

	TM 1	
NaK 78	TT**PEWVKFCRQLFGGFSMLLWIGAILCFLAYGIQ**	
srCa: 46	GK**SLWELVIEQFEDLLVRILLLAACISFVLAWFE**	
	M1M2 loop	
NaK: 112	AATEEEPQNDNLY	loop backbone from pdb2lhb: M88-N100
srCa: 80	EGEETI---TAFV	
	TM 2	
NaK: 125	**LGVVLSAVVIITGCFSYYQEAKS**	
srCa: 90	**EPFVILLILIANAIVGVWQERNA**	
	TM 3	
NaK: 274	**QTPIAAEIEHFIHIITGVAVFLGVSFFI**	
srCa: 246	**KTPLQQKLDEFGEQLSKVISLICVAVWL**	
	M3M4 loop	
NaK: 302	**LS**LILE----------**YTWLE**	loop backbone from pdb1opb: Y[A19]-T[A29]
srCa: 274	**IN**IGHFNDPVHGGSWIRGA**IY**	
	TM 4	
NaK: 313	**AVIFLIGIIVANVPEGLLATVTVCL**	
srCa: 295	**YFKIAVALAVAAIPEGLPAVITTCL**	
	TM 5 **M5M6 loop**	
NaK: 760	**IFDNLKKSIAYTLTSNIPEITPFLIFIIA**NIPLPL	
srCa: 753	**IYNNMKQFIRYLISSNVGEVVCIFLTAAL**GLPEAL	
	TM 6 (continued from TM5) **M6M7 cytoplasmic loop**	
NaK: 796	**GTVTILCIDLGTDMVPAISLAY**EQAESDIMKKRPRNPKTDKL	
srCa: 788	**IPVQLLWVNLVTDGLPATALGF**NPPDLDIMDRPPRSPKEPLI	
	TM 7 (continued from TM6)	
NaK: 838	**VNERLISMAYGQIGMIQALGGF**FTYFVILAEN	
srCa: 830	**SGWLFFRYMAIGGYVGAATVGA**AAWWFMYAED	
	TM 8	
NaK: 906	**IVEFTCHTPFFVTIVVVQWADL**VICK	
srCa: 894	**PEPMTMALSVLVTIEMCNALNS**LSEN	
	M8M9 cytoplasmic loop	
NaK: 932	TRRNSSVFQQGMKN	loop backbone from pdb2lhb: M88-N100
srCa: 920	QSLMRMPP---WVN	
	TM 9 (continued from TM8) **M9M10 loop**	
NaK: 945	**KILIFGLFEETALAAFLSYC**PGMGVALRMYPL	
srCa: 931	**IWLLGSICISMSLHFLILYV**DPLPMIFKLKAL	
	TM 10 (continued from TM9)	
NaK: 977	**KPTWWFCAFPYSLLIFVYDEVRKLII**	
srCa: 963	**DLTQWLMVLKISLPVIGLDEILKFIA**	

constructed by using the three-dimensional (3D) coordinates of the sarcoplasmic reticulum (sr) Ca^{2+}-ATPase (PDB entry 1EUL) as a starting framework. All model building and energy minimizations were performed with Discover and Insight II molecular modeling software by MSI Inc. (San Diego, CA). The subdomains designated P, N, and A in the cytoplasmic domain of the sr Ca^{2+}-ATPase are likely to be structurally homologous in all P2-type ATPases, and these were not altered. The N and A subdomains are distant from the membrane and were held fixed during energy minimizations.

Side chains from the Na^+,K^+-ATPase pig α1 sequence were mapped onto the equivalent positions in the membrane domain of the sr Ca^{2+}-ATPase structure and are identified by a combination of computer and manual sequence alignments. Where differences occurred in the number of residues between aligned membrane segments, the sr Ca^{2+}-ATPase loops in the 3D structure were replaced by using the "search loop" command provided in the software. This subroutine searches a defined set of high-resolution database proteins for loops of a designated size whose pre- and postloop α-carbons closely overlap those of the target structure.

Matching segments from the Na^+,K^+-ATPase α1 sequence (Swiss-Prot accession number P05024) used for replacement of rabbit sr Ca^{2+}-ATPase residues (Swiss-Prot accession number P04191) are given in Table 1 with bold characters indicating regions of a helix. The Ca^{2+}-ATPase residues from Gly[G862] to Ala[A893] (e.g., the M7M8 luminal loop) were left unaltered because the loop size and lack of sequence homology made modeling unfeasible. The region enclosing TM5, the M5M6 luminal loop, TM6, the M6M7 cytoplasmic loop, and TM7 has numerous functional amino acid homologies and an equivalent number of residues in Na^+,K^+- and sr Ca^{2+}-ATPases, and the fragments were therefore replaced throughout. Similarly, TM9 and TM10 have the same number of residues, and no loop replacement was required.

The conformations of substituted side chains were assigned to mimic the volumes of the corresponding sr Ca^{2+}-ATPase residues where possible. Overlapping side chain densities were resolved by assigning only those dihedrals found in known high-resolution helices. Then energy minimization (molecular mechanics) was performed using the consistent valence force field provided with the software to an average absolute derivative of approximately 0.1 kcal mol^{-1} $Å^{-1}$. Sodium ions were placed in the positions occupied by the two calcium ions in sr Ca^{2+}-ATPase, and a third sodium was modeled in the space above Glu309 and between helices M4 and M6. Energy minimization was then repeated to an average absolute derivative of 0.1 kcal mol^{-1} $Å^{-1}$. After minimization, the positions of the membrane helices were only slightly changed in the Na^+,K^+-ATPase model compared to those in the sr Ca^{2+}-ATPase with an rms deviation

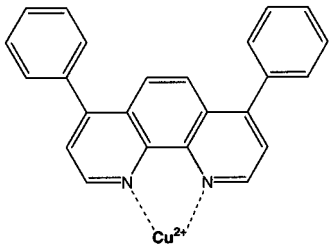

FIGURE 1: Complex (1:1) of 4,7-diphenyl-1,10-phenanthroline with a Cu^{2+} ion.

in the backbones of all the membrane helices (2008 atoms) of 1.519 Å.

Materials. For sodium dodecyl sulfate−polyacrylamide gel electrophoresis (SDS−PAGE), all reagents were electrophoresis-grade from Bio-Rad. Tris (ultrapure) was from Bio Lab (Jerusalem, Israel). L-(+)-Ascorbic acid (catalog number 100127) and 30% H_2O_2 (catalog number 822287) were from Merck. Desferrioxamine mesylate (desferal) (D9533) and ouabain (O3125) were from Sigma. Diethyl pyrocarbonate (DEPC) was obtained from Sigma. Other reagents were analytical-grade. Choline chloride was recrystallized from ethanol. DPP and other phenanthrolines were obtained from Aldrich. The following stock solutions of phenanthrolines were prepared: 4,7-diphenyl-1,10-phenanthroline (DPP), 3,4,7,8-tetramethyl-1,10-phenanthroline (TMP), and 2,9-dimethyl-1,10-phenanthroline (neocuproine) in ethanol, 1,-10-phenanthroline (*o*-phenanthroline) and 4,7-diphenyl-1,10-phenanthrolinedisulfonic acid (DPP-DS) in water, and 2,9-dimethyl-4,7-diphenyl-1,10-phenanthroline (DMDPP) in dimethylformamide (DMF).

RESULTS

Figure 1 depicts the structure of the complex Cu^{2+} ion and 4,7-diphenyl-1,10-phenanthroline (DPP) in a 1:1 ratio. Figure 2 depicts cleavage patterns observed in the presence of Cu^{2+} ions, ascorbate, H_2O_2, and a variety of phenanthrolines, as revealed in immunoblots using anti-KETYY. The phenanthrolines were present in excess (10 μM) over the Cu^{2+} ions (4 μM), to chelate free Cu^{2+} ions. Previously, we described selective Cu^{2+}-catalyzed cleavages of both α and β subunits (*21*), which are suppressed by addition of a chelator like EDTA, leaving an intact α subunit. As seen from lanes 1−5 of Figure 2, which show the results of cleavages in the presence of Cu^{2+} ions and the lipid-soluble phenathrolines, DPP, TMP, or *o*-phenanthroline, these phenanthrolines did not suppress cleavages, as does EDTA, but actually induced the appearance of a variety of fragments. In the case of DPP, the cleavage pattern was very specific, and two large fragments with apparent molecular masses of 96.5 and 76 kDa were observed. In contrast, in the presence of a Cu^{2+}−phenanthroline or Cu^{2+}−TMP complex, a large number of distinct fragments and a nonspecific smear appeared. Six fragments produced by cleavage induced by Fe^{2+}, ascorbate, and H_2O_2, characterized previously (*16*, *19*), serve as convenient markers for locating cleavage induced by Cu^{2+}−phenathroline complexes (lane 5). The 96.5 and 76 kDa fragments produced with the Cu^{2+}−DPP complex have essentially the same mobility as two fragments produced by Fe^{2+}, ascorbate, and H_2O_2 (compare lanes 2 and 5, and see also Figure 4D), but several others were not seen. DPP,

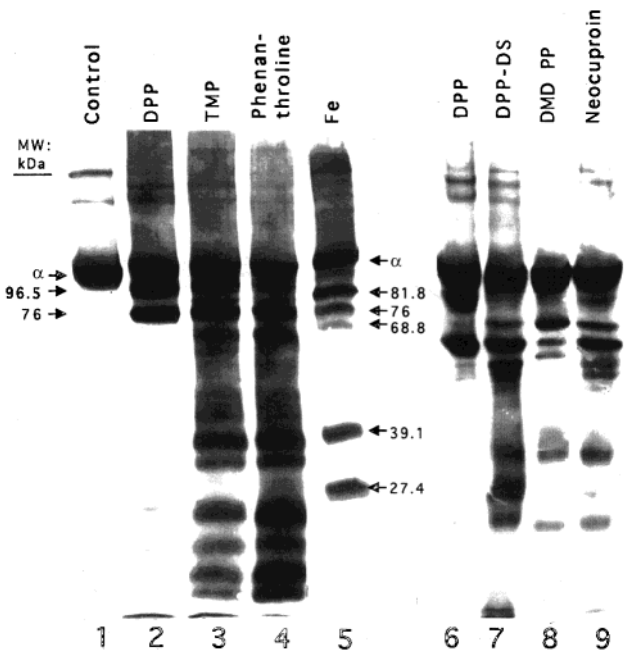

FIGURE 2: Specificity of oxidative cleavages mediated by different phenanthroline derivatives. A suspension of pig kidney Na^+,K^+-ATPase was preincubated for 15 min at 1 mg/mL with $CuCl_2$ (4 μM) and the respective phenanthroline (10 μM). Freshly prepared solutions of ascorbate (4 mM) and H_2O_2 (4 mM) were added; the mixture was incubated for 20 min at 20 °C, and the reaction was arrested by addition of 10 μL of 5-fold concentrated gel sample buffer. The final volume was 60 μL. Electrophoresis on a 7.5% T, 3% C gel, blotting, and immunodetection were carried out as described in Experimental Procedures. The lane labeled Fe refers to a sample of Na^+,K^+-ATPase cleaved with Fe^{2+} cation in a low-ionic strength medium as in ref *19*. The Control lane contained the untreated enzyme.

TMP, and phenanthroline are all hydrophobic, lipid-soluble compounds (phenanthroline < TMP < DPP). Thus, in a second experiment (lanes 6−9), we compared the pattern obtained with the Cu^{2+}−DPP complex to that with the Cu^{2+}−DPP-PS complex, a water-soluble derivative, and the Cu^{2+}−DMDPP complex, an even more hydrophobic derivative than DPP itself. With the Cu^{2+}−DPP-PS complex, some distinct fragments together with a nonspecific smear appeared. With the Cu^{2+}−DMDPP complex, the pattern was typical only for fragments induced by ∼50 nM contaminant Fe^{2+} ions which are always present in the solutions unless they are deliberately chelated (lane 8). A similar pattern was observed in the presence of the Cu^{2+}−neocuproine complex. Neocuproine is a selective Cu^+ chelator, which is so stable that the Cu^+ is not oxidized to Cu^{2+}, making it redox inactive, and thus precluding generation of OH radicals (*25*). In a mixture of Cu^+ and Cu^{2+} ions such as that which exists with ascorbate and H_2O_2, removal of Cu^+ ions will cause the Cu^+−Cu^{2+} equilibrium to reset, so sufficient neocuproine will chelate all of the Cu as Cu^+ ions, leaving only the free contaminant Fe^{2+} ions in solution (lane 9). On the basis of the selective cleavages observed with DPP, one could hypothesize that the Cu^{2+}−DPP complex directs the metal to specific site(s) on the protein where cleavage occurs. In the case of Cu^{2+}−TMP or Cu^{2+}−phen complexes, the targeting could be less selective. The experiments described below tested the hypothesis.

The solution in lane 2 of Figure 2 contained 4 μM added Cu^{2+}, ∼50 nM contaminant Fe^{2+} (*16*), and 10 μM DPP,

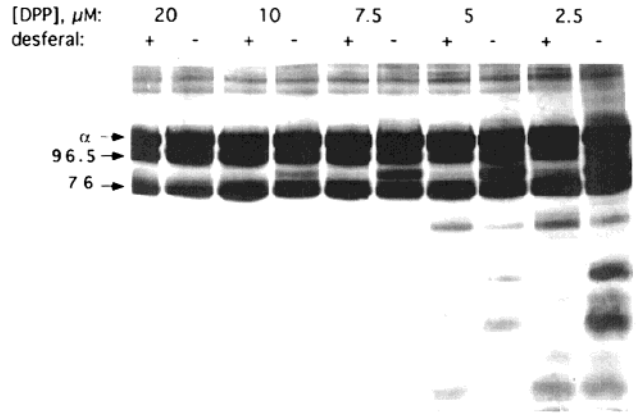

FIGURE 3: Evidence for mediation of selective oxidative cleavages by the Cu^{2+}−DPP complex. The cleavage reaction was carried out in a medium containing 1 μM $CuCl_2$ and 2.5, 5, 7.5, 10, and 20 μM DPP in the presence (+) or absence (−) of 0.1 mM desferal. The incubation time was 90 min.

which binds both Cu^{2+} and Fe^{2+} ions. Due to the excess of DPP in lane 2 of Figure 2, little or no uncomplexed metal ions should remain, and indeed, neither characteristic 12 and 13 kDa fragments generated by free Cu^{2+} ions (*21*) nor the pattern of fragments generated by free Fe^{2+} (lane 5) appeared. In contrast, despite the excess of added Cu^{2+} (4 μM) over contaminant Fe^{2+} (∼50 nM), the possibility that the cleavages were mediated by the Fe^{2+}−DPP complex could not be excluded a priori. In Figure 3 (and Figure 4D), we address the question of the identity of the metal complex catalyzing the cleavages. In Figure 3, the renal enzyme was incubated with ascorbate, H_2O_2, and 1 μM Cu^{2+} together with increasing concentrations of DPP, from 2.5 to 20 μM, in the absence or presence of 50 μM desferal, a highly specific Fe^{3+}/Fe^{2+} chelator, which completely suppresses cleavages mediated by contaminant Fe^{2+} (*16*). At the lowest concentration of DPP (2.5 μM), in the absence of desferal, we observed the 96.5 and 76 kDa fragments and in addition several bands which can be attributed to uncomplexed Fe^{2+} or Cu^{2+}. The presence of desferal completely suppressed the bands produced by Fe^{2+}-catalyzed cleavage, leaving intact the bands at 96.5 and 76 kDa and two additional minor bands which can be attributed to uncomplexed Cu^{2+} ions. As the DPP concentration was progressively increased, the 96.5 and 76 kDa fragments remained while all the other fragments were progressively suppressed, even in the absence of desferal. In the presence of desferal, the bands generated by Fe^{2+}-catalyzed cleavage were always suppressed. At 20 μM DPP, we detected only the 96.5 and 76 kDa fragments, and there was no difference with or without desferal. Clearly sufficient DPP by itself fully complexed all of the free Cu^{2+} or contaminant Fe^{2+}, suppressing cleavages caused by them. Since desferal must have competed with DPP for Fe^{2+} and reduced the concentration of any Fe^{2+}−DPP complex existing in its absence, the lack of an effect of desferal on the yield of 96.5 and 76 kDa fragments shows that they are generated primarily and perhaps only by the Cu^{2+}−DPP complex (see also Figure 4D).

Figure 4 presents data on kinetic features of the Cu^{2+}−DPP-dependent cleavage, which support the assumption of a site-specific mechanism. In panels A and B of Figure 4, it may be seen that the 96.5 and 76 kDa fragments appeared in parallel over time and at increasing concentrations of Cu^{2+}

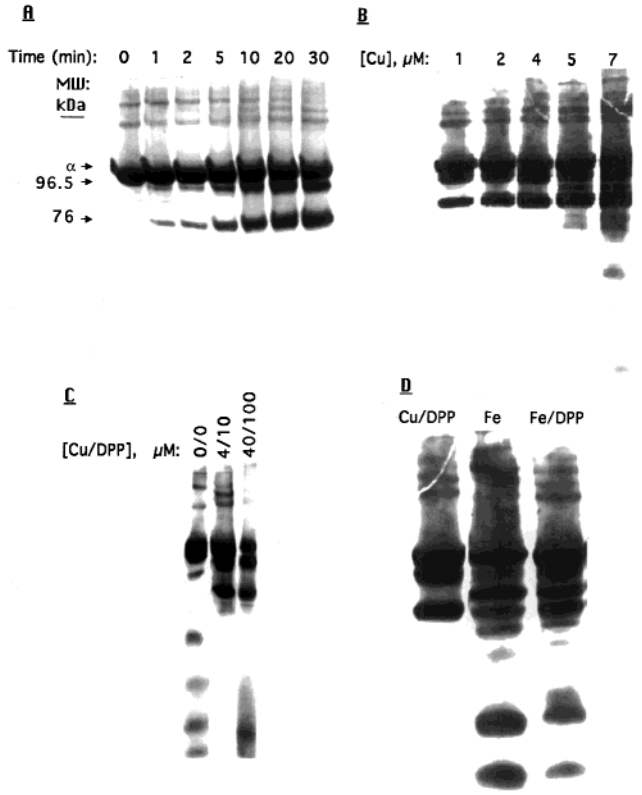

FIGURE 4: Kinetic evidence for a site-specific mechanism of oxidative cleavage. (A) Time course of a cleavage reaction in a medium containing 4 μM $CuCl_2$, 10 μM DPP, 4 mM ascorbate, and 4 mM hydrogen peroxide. (B) Cu−DPP-induced cleavage with 10 μM DPP and increasing concentrations of $CuCl_2$, from 1 to 7 μM, and an incubation time of 5 min. (C) Cleavage at different Cu and DPP concentrations: 0 and 0 μM, 4 and 10 μM, and 40 and 100 μM, respectively (incubation time of 15 min). (D) Cleavage with the Cu−DPP complex (4 and 10 μM, respectively), $FeSO_4$ (4 μM), and the $FeSO_4$−DPP complex (4 and 10 μM, respectively), with an incubation time of 5 min.

ions, i.e., of the Cu^{2+}−DPP complex, consistent with both cleavages being mediated from one site. Figure 4C shows little or no difference in the cleavages with a 10-fold difference in Cu^{2+}−DPP concentration (4:10 and 40:100 Cu^{2+}:DPP ratios, respectively), implying saturation of a site. Figure 4D shows that whereas the combination of Cu^{2+} and DPP selectively generates the 96.5 and 76 kDa fragments, a similar combination of Fe^{2+} and DPP is much less effective (compare the 96.5 and 76 kDa fragments, lanes 1 and 3) and DPP partially reduced the amount of fragments generated by uncomplexed free Fe^{2+}. Another strong indication of a site-specific mechanism is that the cleavages were not affected by the presence of OH radical scavengers (formate or butyl alcohol) in the medium (not shown).

A further indication of selectivity of cleavage mediated by DPP is provided by the experimental results depicted in Figure 5 showing a comparison of immunoblots which use either the standard anti-C-terminal antibody, anti-KETYY, or an antibody, "anti M1/2", which recognizes epitopes within residues 68−168 of the α subunit (*13*, *16*). In the latter case, we observed fragments with apparent molecular masses 33 and 13 kDa which, presumably, are N-terminal fragments complementary to the 76 and 96.5 kDa fragments, respectively, but no other significant fragments. A preparative gel of Na^+,K^+-ATPase extensively cleaved with ascorbate and H_2O_2 and the Cu^{2+}−DPP complex was stained with

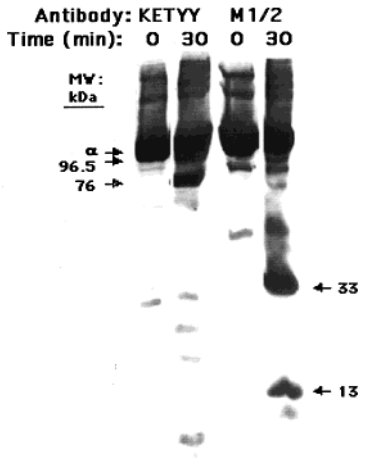

FIGURE 5: Selectivity of cleavages demonstrated by detection of complementary C-terminal and N-terminal fragments. Cleavage of Na^+,K^+-ATPase (1 mg/mL) with Cu^{2+} (4 μM) and DPP (10 μM), incubated at room temperature for 0 or 30 min with ascorbate-Tris (4 mM) and H_2O_2 (4 mM). Bands were detected by blotting with anti-KETYY (C-terminus, two lanes from the left) and with anti-M1/2 (N-terminus, two bands from the right).

Coomassie blue and revealed the 96.5, 76, and 33 kDa fragments (not shown). After a transfer to PVDF paper, we attempted to sequence these fragments. The N-terminus of the 33 kDa fragment was found to be GRDK, as expected for the N-terminus of the α subunit. No sequence was obtained for the 96.5 and 76 kDa fragments, which have blocked N-termini. The gel confirms the inferences from Figure 5, and in particular, it shows that no other fragments were produced in significant quantities. Another indication of the specificity of the Cu^{2+}−DPP-catalyzed cleavage is that neither the β nor the γ subunits were cleaved (not shown).

The mobility of the prominent 76 kDa fragment generated with the Cu^{2+}−DPP complex is indistinguishable from that of the 76 kDa fragments produced by free Fe^{2+}, and that at 96.5 kDa is also close to the highest-M_r fragment produced by free Fe^{2+} (although resolution is worse here) (*16*, *19*). On the basis of their sizes, the N-termini of the 76 and 96.5 kDa fragments must be located near the entrance to transmembrane segments M3 and M1, respectively. We proposed previously that an HFIH sequence at the entrance of M3 could recognize the Fe^{2+} (*16*, *19*). One indication of the involvement of a histidine residue(s) was provided by the finding that pretreatment of the kidney enzyme with the histidine-specific reagent, DEPC, suppresses both Cu^{2+}−DPP-induced cleavages (Figure 6). A second indication came from a comparison of cleavage of the kidney enzyme consisting exclusively of the α1 isoform with the HFIH sequence and cleavage of rat brain axolemma membranes, which contains primarily α2 and α3 isoforms in which the second histidine of HFIH is replaced with glutamine, i.e., HFIQ (*26*, *27*). Figure 7 shows that no cleavages were seen when the axolemma enzyme was incubated with ascorbate, H_2O_2, and the Cu^{2+}−DPP complex, by contrast with the usual 96.5 and 76 kDa fragments, seen with the kidney enzyme. The result depicted in Figure 7 suggests strongly that the second histidine is involved in the Cu^{2+}−DPP-induced cleavages (see the Discussion). A minor 5.5 kDa fragment seen here is addressed further in Figures 8 and 9 below.

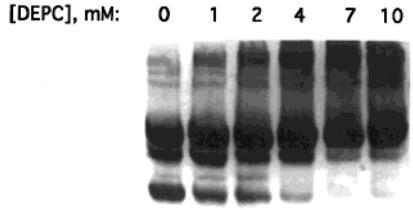

FIGURE 6: Histidine reagent DEPC suppresses Cu^{2+}−DPP-mediated cleavages. Prior to the cleavage reaction, six samples of Na^+,K^+-ATPase were treated with different concentrations (0, 1, 2, 4, 7, and 10 mM) of a fresh solution of DEPC in anhydrous ethanol at room temperature for 30 min. The reagent was removed by centrifuging the membranes and resuspended in a 20 mM HEPES/KOH buffer (pH 7.0). These membranes were used for the cleavage reaction under the following conditions: Na^+,K^+-ATPase (1 mg/mL) with Cu^{2+} (4 μM), DPP (10 μM), incubated at room temperature for 30 min with ascorbate-Tris (4 mM) and H_2O_2 (4 mM).

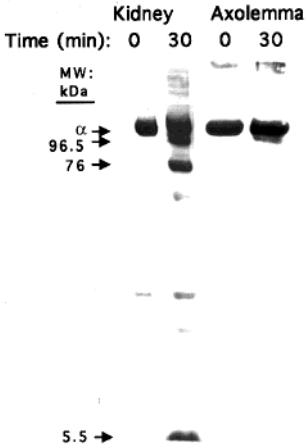

FIGURE 7: Comparison of Cu^{2+}−DPP-mediated cleavage of renal and brain axolemma Na^+,K^+-ATPase. Incubation (0 and 30 min) of Cu^{2+}−DPP-induced cleavage fragments of Na^+,K^+-ATPase from two sources: pig kidney and rat brain axolemma. The other conditions were as described in the legend of Figure 2.

The experiment in Figure 8 examined effects of pump ligands that stabilize different conformational states on the cleavages induced by the Cu^{2+}−DPP complex. Either E_1 or E_2 conformations are stabilized under the different conditions, as follows: low ionic strength, E_2; K^+, (E_2K); Na^+, E_1Na; choline, E_1; Mg^{2+}, E_2; Mg^{2+}/ouabain, E_2.ouabain.Mg; Mg^{2+}/P_i, E_2−P.Mg; and ouabain/P_i/Mg, E_2−P.ouabain (*28*, *29*). There are two principal findings. First, there was little if any effect of any ligand on the yields, absolute or relative, of the 96.5 and 76 kDa fragments. The Cu^{2+}−DPP complex affected neither Na,K-ATPase activity nor Rb occlusion (unpublished results), implying that the complex does not itself stabilize any conformation. The second finding is that a 5.5 kDa fragment was observed in medium containing K^+ ions, Mg^{2+}/ouabain, or especially with Mg^{2+}/P_i and Mg^{2+}/P_i/ouabain complexes. All of these combinations of ligands stabilize E_2 conformations. This 5.5 kDa fragment was also seen sometimes as a minor fragment in the standard low-ionic strength medium (as, for example, in Figure 7). The presence of vanadate ions suppressed all cleavages even without Mg^{2+} ions, suggesting that vanadate may displace the Cu^{2+} ions from the DPP (not shown). The cleavage position of the 5.5 kDa fragment was estimated approximately by comparingits mobility with that of small fragments

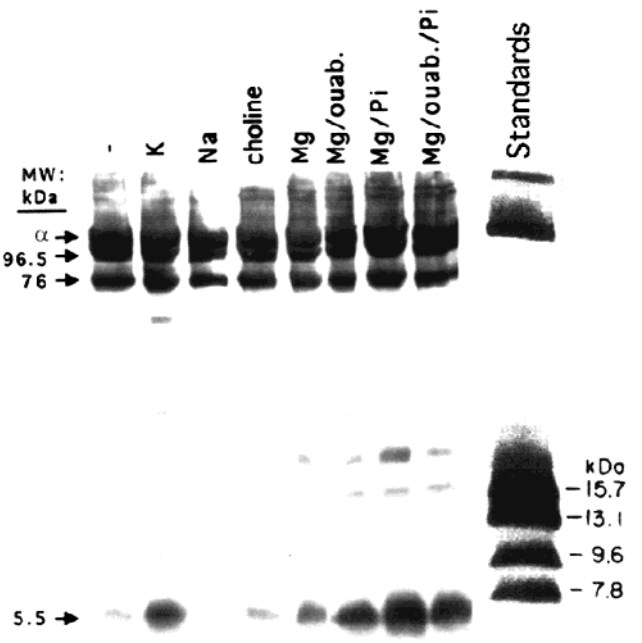

FIGURE 8: Cu^{2+}−DPP-mediated cleavages in different conformational states. The cleavage conditions were as described in the legend of Figure 2 (lane 2) with the addition of the following pump ligands: (from the left) none **(**−**)**, 100 mM KCl **(**K**)**, 100 mM NaCl **(**Na**)**, 100 mM choline chloride **(**choline**)**, 5 mM $MgCl_2$ **(**Mg**)**, 5 mM $MgCl_2$ and 1 mM ouabain **(**Mg/ouab.**)**, 5 mM $MgCl_2$ and 2 mM Tris-phosphate **(**Mg/Pi**)**, and 5 mM $MgCl_2$, 2 mM Tris-phosphate, and 1 mM ouabain **(**Mg/ouab./Pi**)**. The lane marked Standards was scanned from an immunoblot from a chymotryptic digest (Figure 4 of ref *24*). The scan was aligned with the other lanes of the present experiment so as to produce equivalent mobilities of the α subunits.

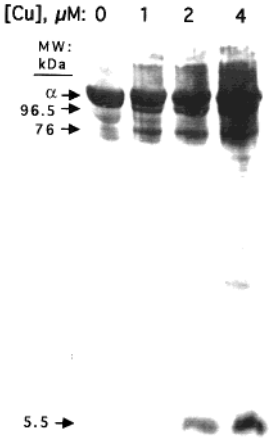

FIGURE 9: Cu^{2+} concentration dependence of Cu^{2+}−DPP-mediated cleavage in an E_2−P.Mg conformation. Cleavages of Na^+,K^+-ATPase (1 mg/mL) with Cu^{2+} (0, 1, 2, or 4 μM) and DPP (10 μM) in a 10 mM Tris-HCl buffer (pH 7.5) containing $MgCl_2$ (5 mM) and Tris-P_i (2 mM). The incubation time was 30 min.

of the α subunit cleaved by chymotrypsin at the extracellular surface (lane marked Standards) (*24*). The 5.5 kDa Cu−DPP-induced fragment runs slightly ahead of a 7.8 kDa chymotryptic fragment which was shown previously to have an N-terminal ^{972}RMYPLK sequence, within the extracellular loop between transmembrane segments M9 and M10 (*24*). Thus, the N-terminus of the 5.5 kDa fragment must lie ∼20 residues downstream of Arg972, which is near the cytoplasmic entrance of M10. A final experiment (Figure 9) looked at the dependence on Cu^{2+} concentrations of the cleavages in the presence of the Mg^{2+}−P_i complex, a condition in which the 5.5 kDa fragment is most prominent (Figure 8). Clearly, the amounts of all three fragments (96.5, 76, and 5.5 kDa) increased in parallel as the Cu^{2+} ion concentration was increased from 1 to 2 and then 4 μM.

DISCUSSION

The results presented show that, in the presence of ascorbate and H_2O_2, the complex of Cu^{2+} and DPP is able to catalyze specific cleavages of the α subunit of Na,K-ATPase. Cu^{2+}−phenanthroline complexes have been used extensively to cleave DNA (*25*), and Cu^{2+} complexed to phenanthroline, covalently bound to engineered cysteine residues, was used to cleave lac permease (*30*); however, cleavage of a membrane protein mediated by a noncovalently bound complex of Cu^{2+} and a hydrophobic phenanthroline has not been described previously.

A Site-Specific Mechanism of Cu^{2+}−DPP-Catalyzed Cleavage. The characteristics of the cleavages induced by the Cu^{2+}−DPP complex indicate that they occur by a site-directed mechanism in which the Cu^{2+} is bound at specific location(s) on the protein, and catalyzes the generation of OH radicals, or a metal−peroxyl intermediate, which cleave the peptide backbone near the site of their generation. The features which suggest strongly that the 96.5 and 76 kDa fragments are cleaved at the same site include (a) the specificity of cleavage, (b) the parallel time course of appearance, (c) the similar Cu^{2+} (i.e., Cu^{2+}−DPP complex) concentration dependence, (d) evidence of a saturation phenomenon, (e) the lack of an effect of OH radical scavengers, (f) the absence of both cleavages in α2 and α3 isoforms in axolemma in which Gln replaces the second His in the HFIH sequence of the renal α1 isoform, and (g) the parallel disappearance of both 96.5 and 76 kDa fragments upon treatment with DEPC. As we have discussed previously in relation to cleavages catalyzed by Fe^{2+} or Cu^{2+} ions, the kinetic properties of site-specific mechanisms imply that each polypeptide chain is cleaved once with a probability which depends, to a first approximation, on the proximity of the cleavage position to the Cu^{2+}−DPP complex, and upon cleavage of the chain, no further cleavages occur (*16*−*21*). The prominence of the fragments is in the order 76 kDa > 96.5 kDa, and so, presumably, this could be the order of proximity to the bound Cu^{2+} ion. The greatest prominence of the 76 kDa fragment fits well with the evidence in Figure 7 which shows that the HFIH sequence is involved in recognition of the Cu^{2+} ion. The evidence regarding the 5.5 kDa fragment is less clear-cut. On one hand, the parallel appearance of the 5.5 kDa fragment with the 96.5 and 76 kDa fragments in Figure 9 is compatible with cleavage mediated by the same Cu^{2+}−DPP complex. On the other hand, the different response to pump ligands of the cleavages producing the 96.5 and 76 kDa, or 5.5 kDa, fragments could imply that a separate Cu^{2+}−DPP complex is involved (see Figure 8).

The Cu^{2+} ion in complexes normally has six ligands. Thus, in solution the Cu^{2+} may form complexes with phenanthroline moieties of up to three DPP molecules, or one or two DPP molecules together with the appropriate number of water molecules. To explain how a complex of Cu^{2+} and DPP is

able to recognize a site or sequence on the protein, we assume that a Cu^{2+} binding center on a protein surface, for example, N atoms of the imidazole ring of histidine residues, replaces ligating groups provided by one or more phenanthroline or water molecules. This should produce a mixed protein−Cu^{2+}−phenanthroline complex. It is analogous to the mixed complexes produced when His tag-labeled proteins are adsorbed onto Ni^{2+}/EDTA columns (protein-His/Ni^{2+}/EDTA column). Depending on the selectivity of the interaction of the Cu^{2+}−phenanthroline complex with the protein, the specificity of the cleavages should change. Because DPP is a highly hydrophobic molecule, it should partition largely into the lipid bilayer, and remove the Cu^{2+} from the aqueous medium. Since, to generate OH radicals, the Cu^{2+} ion must undergo reduction and oxidation by ascorbate and H_2O_2 in the aqueous medium, presumably it is only Cu^{2+}−DPP−protein complexes at the membrane−water interface which can undergo the Fenton chemistry. Thus, the specificity of the cleavages catalyzed by the Cu^{2+}−DPP complex may be the result of its confinement to the membrane−water interface and interaction only there with the appropriate residues, for example, the HFIH sequence near M3. In contrast, less hydrophobic compounds such as *o*-phenanthrolines or TMP or water-soluble derivatives such as DPP-PS should not be confined to the lipid bilayer and may allow the complexed Cu^{2+} to interact with more than one site on the protein, leading to less selective or nonselective cleavages. Why the even more hydrophobic derivative DMDPP is an ineffective catalyst of cleavages is unclear, but it may be significant that the two methyl groups of this phenanthroline are in the same 2 and 9 positions as those in neocuproine, which complexes Cu^{+} so stably as to make it incapable of generating OH radicals by Fenton reactions.

Although the exact positions of the N-termini of the 96.5, 76, and 5.5 kDa fragments in the sequence of the α subunit were not obtained, approximate positions can be assigned as near the cytoplasmic entrance of M1 and M3 and in M10, respectively. One indication comes from the apparent M_r values themselves. A second indication comes from comparison with proteolytic fragments with known N-termini and intact C-termini. For example, we showed previously that the 76 kDa fragment produced with Fe^{2+}, ascorbate, and H_2O_2, with mobility indistinguishable from that of the Cu^{2+}−DPP-catalyzed 76 kDa fragment, is located ∼10 residues downstream of the N-terminus of a chymotryptic fragment at Ile266, which is near the ^{283}HFIH sequence at the entrance of M3 (*19*). In support of this assignment, the second histidine in the ^{283}HFIH sequence is strongly implicated by the lack of Cu^{2+}−DPP-catalyzed cleavages in the axolemma membranes containing primarily α2 and α3 isoforms with glutamine replacing the second histidine (Figure 7). With regard to the 5.5 kDa fragment, as shown in Figure 8, comparison of its mobility with that of a 7.8 kDa chymotryptic fragment (N-terminal Arg972; see ref *24*) shows that its N-terminus must lie near the cytoplasmic end of M10. Finally, these assignments, at the cytoplasmic entrance of M1, M3, and M10, are consistent with the requirement that cleavages occur at a membrane−water interface.

Comparison of Fe^{2+}-catalyzed cleavages with the Cu^{2+}−DPP-catalyzed cleavages leads to an important conclusion regarding the former. Of the six Fe^{2+}-catalyzed fragments observed in E_2 conformations, four are suppressed in E_1 conformations while two fragments are unaffected and are observed in both conformations (*16*, *19*). The mobility and insensitivity to the conformational state of these latter two fragments are essentially like those of the two major Cu^{2+}−DPP-catalyzed fragments. Although only one Fe^{2+} site is required to explain the kinetics of the cleavages, as mentioned in the introductory section, the Ca^{2+}-ATPase crystal structure suggests that there are in fact two widely separated Fe^{2+} sites, the conformation-sensitive site 1 in the P and A domains and the conformation-insensitive site 2 near the membrane. However, experimental evidence for two Fe^{2+} sites has not been available until now. Obviously, the fact that cleavages catalyzed by the Cu^{2+}−DPP complex located in the membrane are essentially the same as Fe^{2+}-catalyzed fragments in site 2, but those in site 1 are not observed at all, provides strong experimental support for the concept of two separate Fe^{2+} sites.

Arrangement of Transmembrane Helices. Homology Modeling. We have constructed a homology model with the transmembrane segments of Na^+,K^+-ATPase and short connecting loops substituted for those of Ca^{2+}-ATPase, to make predictions and test inferences based on experimental data, and so obtain evidence for similarities and differences in the transmembrane organization of the two pumps (details in Table 1 and Experimental Procedures). Of course, the homology model cannot take into account any influence of the β subunit, which might affect the fold in the region of strong α−β subunit interactions near M8. Nevertheless, the model allows us to test the predictions of cleavage experiments and compare helix packing of Na^+,K^+-ATPase and Ca^{2+}-ATPase based on cleavage experiments.

The left panel of Figure 10 depicts the backbone of the "chimeric" molecule with Na^+,K^+-ATPase residues in color and Ca^{2+}-ATPase residues in gray and the right panel of Figure 10 an expanded view of the transmembrane region. Not surprisingly, the structure is quite similar to the real Ca^{2+}-ATPase structure. As seen in Figure 10, although the M3 and M1 transmembrane segments are tilted with respect to each other, they come close to each other near the cytoplasmic membrane surface. In this respect, they are quite similar to M3 and M1 of Ca-ATPase. The more important point is that the greatest proximity occurs between the HFIH sequence on M3 and the EWVK sequence before M1, and furthermore, the interacting surfaces are oriented outward toward the lipid, where the Cu^{2+}−DPP complex should be located. The two histidines of the HFIH sequence and the opposing glutamate of the EWVK sequence could form a cage to ligate a heavy metal ion between them. In other proteins, ligation of a heavy metal ion by the triangular arrangement of HXXH and a glutamate has been described (*31*). Obviously, the model strongly supports the proximity of M3 and M1 predicted by cleavages catalyzed by the Cu^{2+}−DPP complex (or by Fe^{2+} in its site 2). Conversely, the cleavage experiments provide evidence for similar packing of M3 and M1 of Na^+,K^+-ATPase and Ca^{2+}-ATPase. The model also provides a rough estimate of the spatial resolution of the cleavage technique. The distance between the peptide backbone and an Fe^{2+} ion placed between the two histidines and the glutamate is 6−10 Å. In contrast, the distance to the backbone of the loop L6/7 which makes a contact with M3, but is not cut at all, is ∼14 Å.

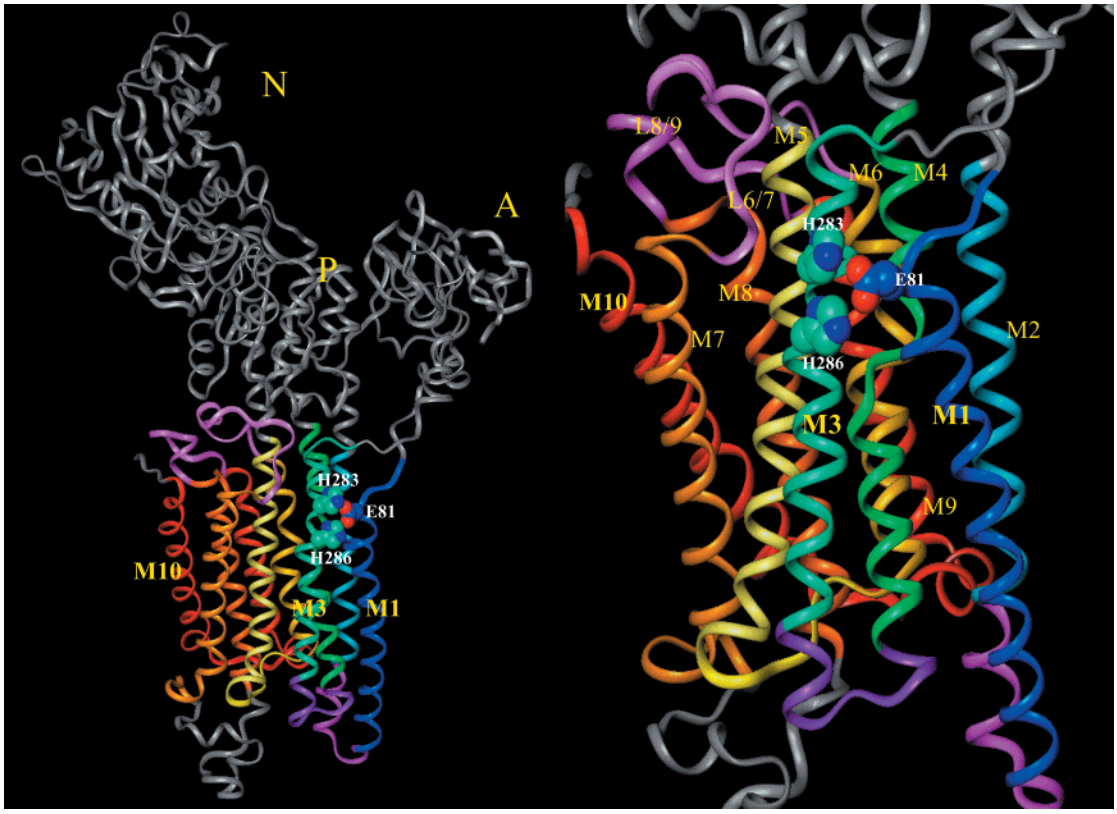

FIGURE 10: Homology model based on the Ca^{2+}-ATPase crystal structure. Transmembrane segments and cytoplasmic loops from the pig α1 Na^+,K^+-ATPase are in color. Ca^{2+}-ATPase residues are in gray. Numbering is as in the pig α1 sequence.

The insensitivity to E_1 or E_2 conformations of the cleavages near M3 and M1 (Figure 8) implies that neither M1 nor M3 moves significantly with respect to each other or the Cu^{2+}−DPP complex at the point of interaction near the cytoplasmic surface. Presumably, therefore, the large movement of the A domain toward the P and N domains which occurs in the $E_1 \rightarrow E_2$ transition involves rotation of the A domain about bonds within the segments connecting it to the M3 and M1 helices. As judged by the "temperature factor" in the crystal structure of Ca^{2+}-ATPase, these connecting segments are in fact among the most flexible in the whole molecule. The result in Figure 8 does not exclude a change in tilt of the M3 and M1 segments. If the latter occurred, this would cause changes in helix packing at the extracellular surface.

In the Ca^{2+}-ATPase structure and the model in Figure 10, M9 and M10 are located on the side of the molecule opposite to M3 and M1. On the basis of our evidence, it is not possible to rule out the possibility that the cleavage to produce the 5.5 kDa fragment is mediated by a Cu^{2+}−DPP molecule separate from that which produces the 96.5 and 76 kDa fragments. In this case, no statements on the proximity of M10 to M3 and M1 can be made. Neither, however, can we absolutely exclude the proximity of M10 to M3 and M1. Since the model does not include the β subunit, Mβ of Na^+,K^+-ATPase (or H^+,K^+-ATPase) might displace the M9/M10 pair from the position next to M8 as in Ca^{2+}-ATPase, and allow M10 to come into proximity with M3 and M1, at least in E_2 conformations for which the cleavage near M10 was most prominent. Obviously, additional experimental evidence is required on the helix packing, especially in the regions of α−β subunit interactions.

CONCLUSIONS

Specific cleavages catalyzed by the Cu^{2+}−DPP complex or by free Fe^{2+} complexed in its site 2 provide a novel way to detect proximities between transmembrane segments. The conclusions concerning the proximity of M3 and M1 are particularly convincing when combined with homology modeling based on the Ca^{2+}-ATPase crystal structure. This approach could be extended to determine the proximity of other transmembrane segments, particularly for regions of α−β subunit interactions, by looking at cleavages in recombinant Na^+,K^+-ATPase, mutated so as to remove the native metal binding site and create new sites at desired locations. The homology model will be important in planning such mutations.

Oxidative cleavages mediated by Fe^{2+} or Cu^{2+} ions at engineered binding sites could of course be utilized to analyze the structural organization of other membrane proteins, including the majority for which no 3D crystal structure or homology modeling is available.

ACKNOWLEDGMENT

S.J.D.K. thanks George Sachs for hospitality on a sabbatical visit in the Department of Physiology, University of California, Los Angeles, CA (January to June 2001), and helpful comments on the manuscript.

REFERENCES

1. Glynn, I. M. (1985) in *Enzymes of Biological Membranes* (Martonosi, A., Ed.) pp 35−114, Plenum Press, New York.
2. Glynn, I. M., and Karlish, S. J. D. (1990) *Annu. Rev. Biochem. 59*, 171−205.

3. Toyoshima, C., Nakasako, M., Nomura, H., and Ogawa, H. (2000) *Nature 405*, 647−655.
4. Geering, K. (1991) *FEBS Lett. 285*, 189−193.
5. Chow, D.-C., and Forte, J. D. (1995) *J. Exp. Biol. 198*, 1−17.
6. Møller, J. V., Juul, B., and Le Maire, M. (1996) *Biochim. Biophys. Acta 1286*, 1−51.
7. Andersen, J. P., and Vilsen, B. (1995) *FEBS Lett. 359*, 101−106.
8. McLennan, D. H., Rice, W. J., and Green, N. M. (1997) *J. Biol. Chem. 272*, 28815−288818.
9. Fambrough, D. M., Lemas, M. V., Kamrick, M., Emerick, M., Renaud, K. J., Inman, E. M., Hwang, B., and Takeyasu, K. (1994) *Am. J. Physiol. 266*, C579−C589.
10. Geering, K. (2000) *J. Membr. Biol. 174*, 181−190.
11. Therien, A. G., and Blostein, R. (2000) *Am. J. Physiol. 279*, C541−C566.
12. Karlish, S. J. D., Goldshleger, R., and Stein, W. D. (1990) *Proc. Natl. Acad. Sci. U.S.A. 87*, 4566−4570.
13. Capasso, J. M., Hoving, S., Tal, D. M., Goldshleger, R., and Karlish, S. J. D. (1992) *J. Biol. Chem. 267*, 1150−1158.
14. Or, E., Goldshleger, R., Shainskaya, A., and Karlish, S. J. D. (1998) *Biochemistry 37*, 8197−8207.
15. Or, E., Goldshleger, R., and Karlish, S. J. D. (1999) *J. Biol. Chem. 274*, 2802−2809.
16. Goldshleger, R., and Karlish, S. J. D. (1997) *Proc. Natl. Acad. Sci. U.S.A. 94*, 9596−9601.
17. Goldshleger, R., Bar Shimon, M., Or, E., and Karlish, S. J. D. (1998) *Acta Physiol. Scand. 163*, 89−98.
18. Bar Shimon, M., Goldshleger, R., and Karlish, S. J. D. (1998) *J. Biol. Chem. 273*, 34190−34195.
19. Goldshleger, R., and Karlish, S. J. D. (1999) *J. Biol. Chem. 274*, 16213−16221.
20. Patchornik, G., Goldshleger, R., and Karlish, S. J. D. (2000) *Proc. Natl. Acad. Sci. U.S.A. 97*, 11954−11959.
21. Goldshleger, R., Patchornik, G., Bar Shimon, M., Tal, D. M., Post, R. L., and Karlish, S. J. D. (2001) *J. Bioenerg. Biomembr.* (in press).
22. Jørgensen, P. L. (1988) *Methods Enzymol. 156*, 29−43.
23. Sweadner, K. J. (1988) *Methods Enzymol. 156*, 65−71.
24. Goldshleger, R., Tal, D. M., and Karlish, S. J. D. (1995) *Biochemistry 34*, 8668−8679.
25. Sigman, D. S., and Chen, C. B. (1990) *Annu. Rev. Biochem. 59*, 207−236.
26. Sweadner, K. J. (1989) *Biochim. Biophys. Acta 988*, 185−220.
27. Munzer, J. S., Daly, S. E., Jewell-Motz, E. A., Lingrel, J. B., and Blostein, R. (1994) *J. Biol. Chem. 269*, 16668−16676.
28. Jørgensen, P. L., and Andersen, J. P. (1988) *J. Membr. Biol. 103*, 95−120.
29. Robinson, J. D., and Pratap, P. R. (1993) *Biochim. Biophys. Acta 1154*, 83−104.
30. Wu, J., Perrin, D. M., Sigman, D., and Kaback, H. R. (1995) *Proc. Natl. Acad. Sci. U.S.A. 92*, 9186−9190.
31. Chang, S. H., Teshima, G. M., Milby, T., Gillece-Castro, B., and Canova-Davis, E. (1997) *Anal. Biochem. 244* (2), 221−227.

BI011167N